Monocytes expressing CX3CR1 orchestrate the development of vincristine-induced pain

Elizabeth A. Old,[1] Suchita Nadkarni,[2] John Grist,[1] Clive Gentry,[1] Stuart Bevan,[1] Ki-Wook Kim,[3] Adrian J. Mogg,[4] Mauro Perretti,[2] and Marzia Malcangio[1]

[1]Wolfson Centre for Age-Related Diseases, King's College London, London, United Kingdom.
[2]The William Harvey Research Institute, Barts and The London School of Medicine, London, United Kingdom.
[3]Department of Microbial Pathogenesis, Yale University School of Medicine, New Haven, Connecticut, USA.
[4]Eli Lilly and Company Ltd., Erl Wood Manor, Windlesham, Surrey, United Kingdom.

A major dose-limiting side effect associated with cancer-treating antineoplastic drugs is the development of neuropathic pain, which is not readily relieved by available analgesics. A better understanding of the mechanisms that underlie pain generation has potential to provide targets for prophylactic management of chemotherapy pain. Here, we delineate a pathway for pain that is induced by the chemotherapeutic drug vincristine sulfate (VCR). In a murine model of chemotherapy-induced allodynia, VCR treatment induced upregulation of endothelial cell adhesion properties, resulting in the infiltration of circulating CX3CR1$^+$ monocytes into the sciatic nerve. At the endothelial-nerve interface, CX3CR1$^+$ monocytes were activated by the chemokine CX3CL1 (also known as fractalkine [FKN]), which promoted production of reactive oxygen species that in turn activated the receptor TRPA1 in sensory neurons and evoked the pain response. Furthermore, mice lacking CX3CR1 exhibited a delay in the development of allodynia following VCR administration. Together, our data suggest that CX3CR1 antagonists and inhibition of FKN proteolytic shedding, possibly by targeting ADAM10/17 and/or cathepsin S, have potential as peripheral approaches for the prophylactic treatment of chemotherapy-induced pain.

Introduction

As our ability to manage the immune and myelosuppression that occurs during cancer treatment with antineoplastic drugs has improved, a secondary dose-limiting side effect of these compounds has been revealed: neurotoxicity (1). Several antineoplastic drugs, including the vinca alkaloids, are able to cause a distal, bilateral, and symmetrical peripheral neuropathy primarily affecting the longest neurons of the extremities, at which they can cross the nerve-blood barrier (2). The neurotoxicity is dependent on cumulative dose protocols, and the severity and progression of the neuropathy correlates with the duration of the treatment. Neuropathy has been reported in an excess of 85% of patients (3) and is the cause of chemotherapy cessation in between 20% (4) and 40% (5) of this population. Pain is the key symptom of this condition and rated as a 7 of 10 in severity by patients (4) who assigned "throbbing," "sharp," and "burning" properties to the pain (6). For those who are able to complete their chemotherapy treatment, pain remains poorly controlled by available analgesics (6), thus prompting preclinical studies aimed at understand the mechanisms underlying the neurotoxicity and its associated pain (7).

Current animal models have begun to approximate to the human condition, including the development of mechanical allodynia and hyperalgesia and cold allodynia — but not heat sensitivity — which can be prevented/reversed by antiepileptic drugs (8, 9). In the preclinical setting, the primary aim is to characterize the initial mechanisms for sensory neuron activation to enable the identification of new therapeutic targets for prophylactic treatment of chemotherapy-induced pain. While several chemotherapeutic agents cause often painful neuropathy, the mechanisms underlying the development of pain might be specific to a class of drug. These drugs share tropism toward peripheral nerves where they can cause axonal damage. Such damage has, however, proved challenging to reproduce in animal models, though the presence of macrophages in peripheral nerves during chemotherapy treatments is suggestive of the occurrence of some degree of injury (10).

Here, we have used a mouse model of chemotherapy-induced allodynia. Specifically, we caused dose-dependent cumulative toxicity using multiple administrations of vincristine sulfate (VCR) to model cancer treatment protocols used in the clinic (11). Peripheral sensory neurons are more susceptible to VCR toxicity than CNS neurons, due to the low activity of P-glycoprotein transporter at the blood-nerve barrier (2). VCR is a substrate for P-glycoprotein, which efficiently limits drug distribution into the brain, where the transporter activity level is high. P-glycoprotein is, however, less efficient in interfering with VCR entry into the peripheral nerves, where the occurrence of macrophage infiltration and release of pronociceptive cytokines indicate local inflammatory damage following VCR administration (12, 13). We show that VCR-induced allodynia is mediated by circulating monocytes, which infiltrate peripheral nerves, and that the control of monocyte-macrophage trafficking and activation may provide preemptive management of vincristine-induced pain.

Results

Vincristine-induced allodynia and the temporal profile of monocytes/macrophages in the sciatic nerve. The administration of VCR for 5 consecutive days (days 0–4; first cycle), followed by a 2-day pause and subsequent treatment for 5 further consecutive days (days 7–11; second cycle) (cumulative dose 5 mg/kg) was associated with hind paw mechanical hypersensitivity (allodynia), which reached

Conflict of interest: The authors have declared that no conflict of interest exists.
Citation for this article: *J Clin Invest.* 2014;124(5):2023–2036. doi:10.1172/JCI71389.

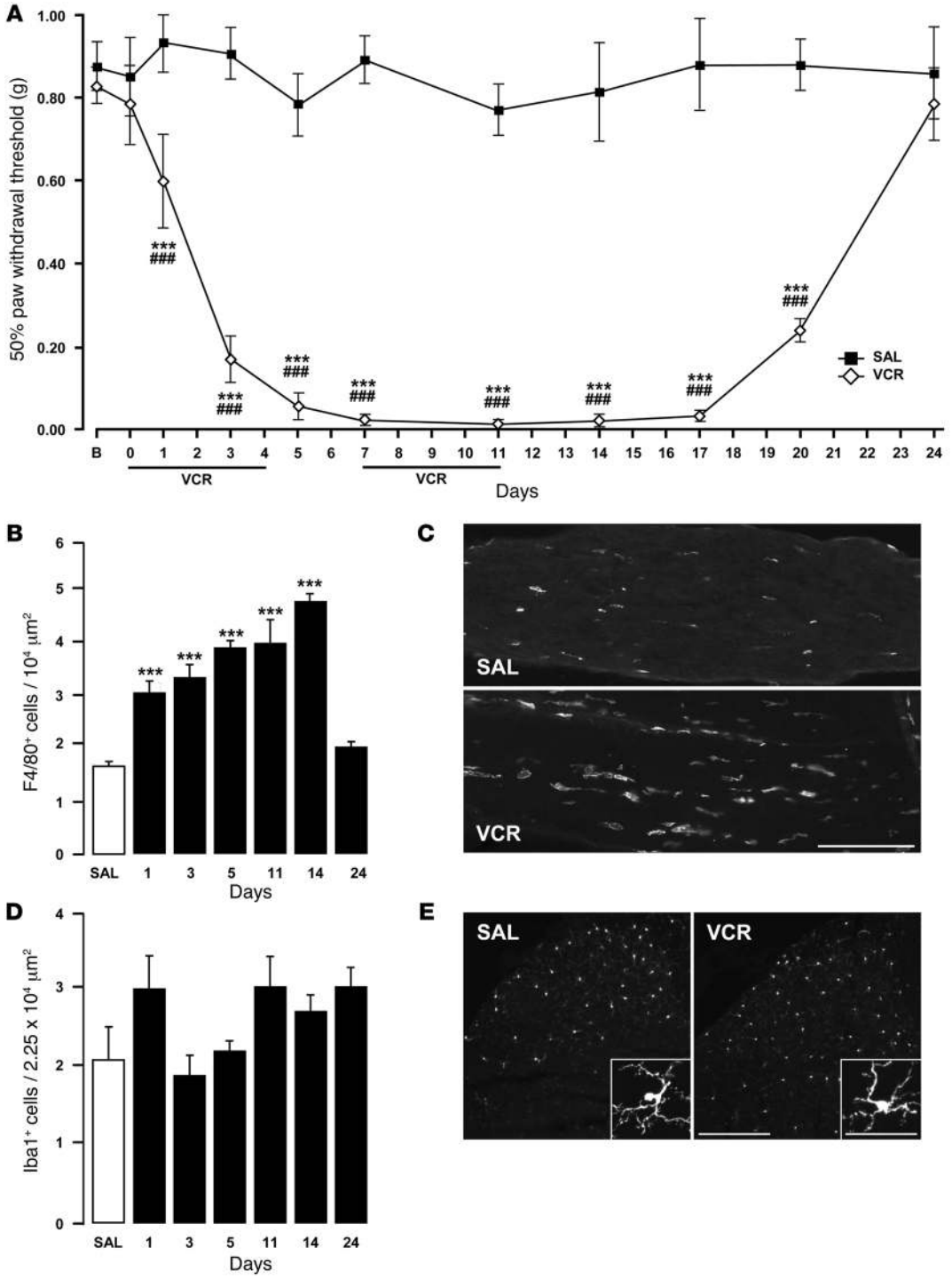

Figure 1

Vincristine treatment induces mechanical allodynia and macrophage infiltration in the sciatic nerve. (**A**) Development of mechanical allodynia following VCR administration at 0.5 mg/kg/d i.p. for 2 cycles of 5 days each (days 0–4 and 7–11; black horizontal bars) (total dose 125 μg per mouse). Data are expressed as 50% of paw withdrawal thresholds (mean ± SEM; saline vehicle group, n = 8 mice; VCR group, n = 12 mice [day 24, n = 6]). ***P < 0.001 compared to baseline thresholds (B), ###P < 0.001 compared saline-treated thresholds, 2-way RM ANOVA, post-hoc Holm-Sidak test. (**B**) Significant monocyte-macrophage infiltration of the sciatic nerve during and after VCR cycles. The number of F4/80$^+$ cells was counted in 10^4 μm^2 boxes in sciatic nerve segments (mean ± SEM, n = 4 mice). ***P < 0.001 compared to saline control, 1-way ANOVA, post-hoc Tukey test. (**C**) Representative photomicrographs showing F4/80$^+$ cells in sciatic nerve sections after 4-day treatment with saline or VCR. Scale bar: 200 μm. (**D**) No change in microglial cell numbers in the dorsal horn of the spinal cord during and after VCR cycles. The number of Iba1$^+$cells was counted in 2.25 × 10^4 μm^2 boxes (mean ± SEM, n = 4 mice per group). (**E**) Representative photomicrographs of Iba1$^+$ cells in lumbar dorsal horn sections obtained after either saline or VCR treatment for 11 days. Scale bar: 100 μm; 20 μm (insets).

statistical significance 24 hours after the first VCR injection. The hypersensitivity was well established following completion of the first cycle (day 4), maintained through the second cycle (day 7–11), and persisted for 6 days after completion of the second cycle (day 17). The mechanical hypersensitivity then gradually recovered and thresholds reached baseline values by 24 days after the first VCR administration (Figure 1A), resembling the recovery seen in many patients in the clinic (1).

The lumbar dorsal root ganglia (DRG) obtained after completion of either the first VCR cycle (day 4) or the second VCR cycle (day 11) showed a nuclear ATF3 expression, which was comparable to that of control ganglia (percentage of cell bodies $ATF3^+$ per total counts ± SEM: saline, 0.7 ± 0.2; day 4 VCR, 1.9 ± 0.4; day 10 VCR, 1.6 ± 0.4; Supplemental Figure 1; supplemental material available online with this article; doi:10.1172/JCI71389DS1), providing no evidence for discernible peripheral axon damage following cumulative VCR dosing of 125 μg/25 g mouse, as similarly reported for paclitaxel- and oxaliplatin-induced neuropathies (14). Likewise, quantification of the intradermal nerve fiber density in the glabrous skin of the hind paw on VCR days 1, 4, 11, and 17 did not demonstrate significant alterations in density from the approximately 45 fibers per mm observed in control skin samples (Supplemental Figure 2), as reported previously (13). However, the number of monocyte-macrophages in the DRG was increased by approximately 60% following VCR treatment compared with that after saline control treatment (number of $F4/80^+$ cells per 10^4 μm^2: saline group, 4.2 ± 0.11; VCR day 4 [first cycle], 6.48 ± 0.15, $P < 0.001$; VCR day 10 [second cycle], 6.21 ± 0.16, $P < 0.001$; Supplemental Figure 3).

More significantly, in peripheral sciatic nerve sections, the monocyte-macrophage numbers were increased by 100% in VCR-exposed nerves compared with control nerves as soon as 24 hours after the first VCR injection (day 1; Figure 1B). The number of $F4/80^+$ cells increased gradually during and after the VCR first cycle (days 3 and 5; Figure 1, B and C) and was still significantly high at the end of the second cycle (day 11; Figure 1B). This was sustained for a few days after VCR treatment (day 14; Figure 1B), before cell numbers returned to control values by 2 weeks after completion of VCR cycles (day 24) (Figure 1B). Conversely, infiltration of neutrophils (MPO^+ cells) into the nerve was not observed (Supplemental Figure 4). FACS analysis of whole blood samples demonstrated no change in monocyte populations in VCR- and saline-treated mice (Supplemental Figure 5). However, as reported in clinical settings (15), VCR induced marked neutropenia, which was evident from the significant reduction in $Gr\text{-}1^{hi}GFP^-$ cells at days 1 and 4 after VCR commencement (Supplemental Figure 5). In contrast to monocyte-macrophages in the peripheral nerve, both the morphology and number of microglial cells in the lumbar dorsal horn were no different from those of saline-treated controls during and after the first cycle (days 1, 3, and 5; Figure 1D), at the end of the second cycle (day 11 and 14; Figure 1, D and E), and 2 weeks after termination of VCR treatment (day 24; Figure 1D), confirming that microglia, the macrophages of the CNS parenchyma (16), do not respond to chemoneuropathy (17, 18).

These data demonstrate that VCR administration is associated with peripheral macrophage infiltration of the sciatic nerve, but neither discernible neuronal stress nor microglial activation in the spinal cord, with the pattern of macrophage infiltration following the same temporal profile as behavioral allodynia.

VCR-induced allodynia and monocytes/macrophage depletion. To test whether the infiltration of monocyte-macrophages into the sciatic nerve contributes to the development of VCR-induced allodynia, we transiently depleted mice of these leukocytes by 2 administrations of liposome-encapsulated clodronate (LCL) 3 and 1 days before the commencement of the first VCR cycle. We have shown previously that LCL administration results in antihyperalgesic effect in neuropathic animals and concomitant decrease in spleen macrophages and macrophages infiltrating injured nerves for up to 4 days after treatment (19). Here, using FACS analysis of whole blood samples, we quantified the depletion of blood monocytes after 2 LCL administrations and found it to be significant both after LCL treatment alone and after the commencement of VCR treatment subsequent to LCL administration (Supplemental Figure 6).

In contrast to control mice, for which mechanical thresholds gradually decreased with daily VCR dosing, the thresholds of LCL-treated mice remained unaltered for up to 4 injections of VCR (day 3) and started to decrease significantly only after the fifth dose of VCR (day 4) to levels that were still higher than those in vehicle-treated mice (Figure 2A). Thresholds became comparable between the control and LCL groups after completion of the first VCR cycle (day 5) and during the second VCR cycle (days 7–11) (Figure 2A). In concordance with a significant prevention of VCR-induced allodynia, the LCL treatment prevented the accumulation of monocyte-macrophages in the sciatic nerve by the end of the first VCR cycle (day 4) as expected (Figure 2, B and C). However, these cells significantly populated the nerve by the end of the second cycle (day 11) (Figure 2, B and D). This suggests that monocyte-macrophages that invade the sciatic nerve following VCR administration play a critical role in the generation of allodynia following VCR treatment.

VCR-induced allodynia and CX3CR1 monocytes. Mouse monocytes include a population of cells ($Ly6C^{lo}[Gr\text{-}1^-]CX3CR1^{hi}$), which is relatively long-lived and patrols the vessel wall, and a "classical" $Ly6C^{hi}(Gr\text{-}1^+)CX3CR1^{int}$ monocyte population, which is short-lived and rapidly recruited to sites of inflammation (20–22). The physical interaction of CX3CR1 with transmembrane CX3CL1 (also known as fractalkine [FKN]) expressed on endothelial cells is proposed to promote cell survival and leukocyte adhesion in a Giα protein–independent fashion (23). In contrast, ADAM10 or ADAM17 sheddase activity is required for the transmigration of adherent leukocytes through the endothelium (24). The myeloid infiltrate observed in the sciatic nerves of VCR-treated animals is likely to derive from $Ly6C^{hi}(Gr\text{-}1^+)CX3CR1^{int}$ monocyte increase and could release pronociceptive mediators that activate sensory neurons.

We evaluated the development of VCR-induced allodynia and monocyte-macrophage infiltration in the sciatic nerves of *Cx3cr1*-deficient mice (referred to as KO mice throughout). In contrast to WT (littermate control) mice, in which mechanical thresholds gradually decreased following daily VCR administration, reaching a severe allodynia by the fourth injection (day 3), KO thresholds remained unchanged for the duration of the first VCR cycle (days 0–4). Thresholds in the KO mice dropped 24 hours after completion of the first cycle (day 5) and were as low those as in WT during the second VCR cycle (days 7–11) (Figure 3A). Therefore, although KO mice did develop severe mechanical hypersensitivity following systemic administration of VCR, it was significantly delayed compared with that of WT mice. In the sciatic nerves of KO mice, the number of $F4/80^+$ cells remained unaltered following the first VCR cycle (day 4) in contrast to the increased

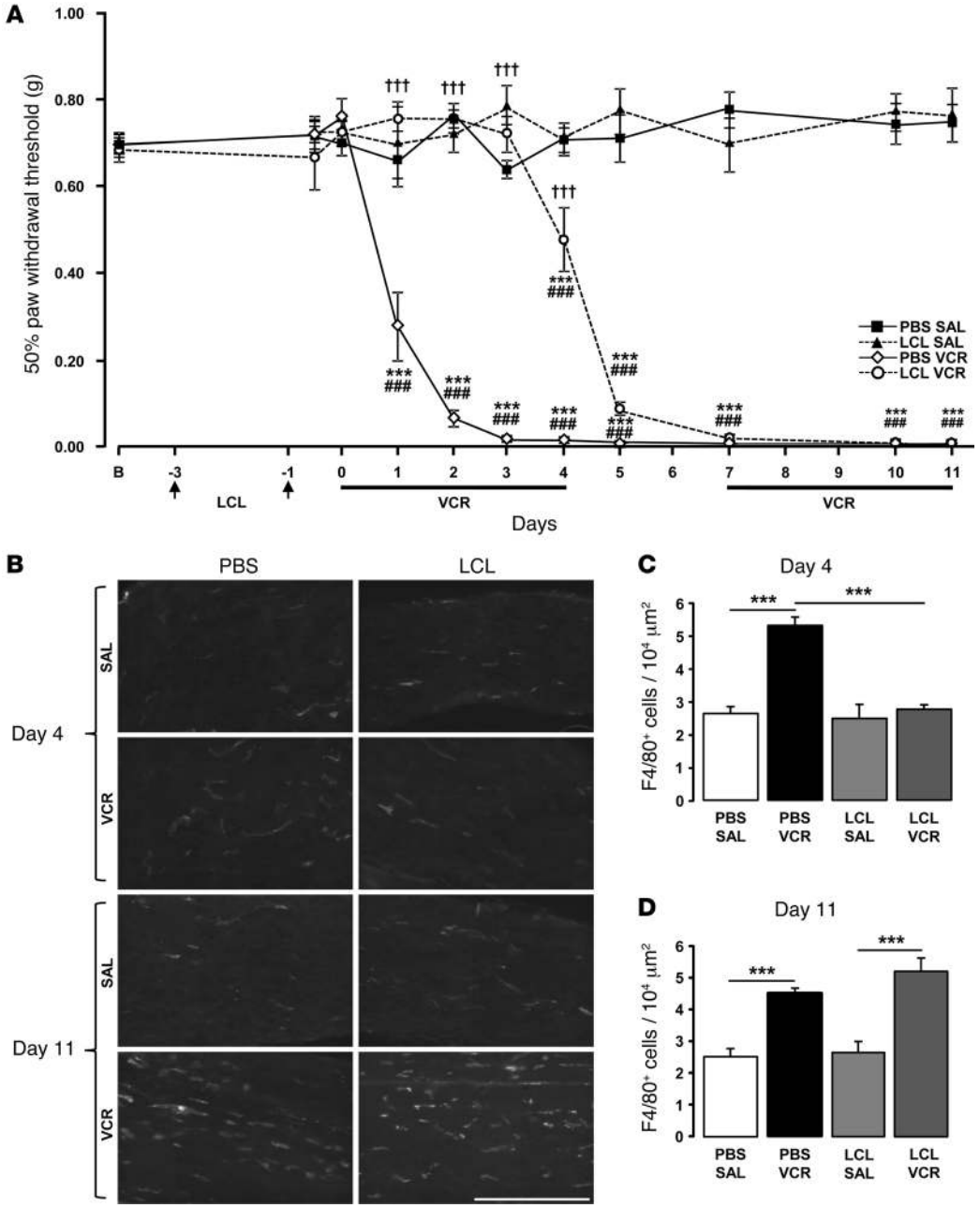

Figure 2

Macrophage depletion prevents vincristine-induced allodynia. (**A**) LCL pretreatment prevents the development of VCR-induced allodynia. LCL (arrows; two 100 μl/10 g injections of 5 mg/ml LCL in PBS i.p.) was injected on day 3 and 1 before VCR (0.5 mg/kg/d i.p. from day 0 to 4; black horizontal bars). Data are expressed as 50% of paw withdrawal thresholds (mean ± SEM) (first VCR cycle, n = 9–11 mice; second VCR cycle, n = 4–6 mice). $^{***}P < 0.001$ compared to baseline thresholds, $^{###}P < 0.001$ compared to saline vehicle, $^{†††}P < 0.001$ compared to PBS+VCR, 2-way RM ANOVA, post-hoc Holm-Sidak test. (**B**) Representative photomicrographs demonstrating that LCL prevents monocyte-macrophage (F4/80$^+$ cell) infiltration in the sciatic nerve by the end of the first VCR cycle (days 0–4) but not the second VCR cycle (days 7–11). Scale bar: 200 μm. (**C** and **D**) The number of F4/80$^+$ cells was counted in 10^4 μm^2 boxes in sciatic nerve segments (mean ± SEM, n = 4 mice per group). $^{***}P < 0.001$, 1-way ANOVA, post-hoc Tukey test.

number of monocyte-macrophages in WT mice (Figure 3, B and C). However, on day 5, when allodynia was apparent, the number of F4/80$^+$ cells in the sciatic nerves of KO mice had increased significantly (Figure 3C). Furthermore, by the end of the second VCR cycle (day 11) when severe allodynia was present in both genotypes, the number of F4/80$^+$ cells in the nerves of KO mice remained significantly increased (Figure 3, B and C). In KO mice, the numbers of Ly6C^{lo}(Gr-1$^-$) monocytes are reduced to 30% and absence of CX3CR1 receptor could also interfere with the survival of macrophages once they are generated from monocytes (23). Our data

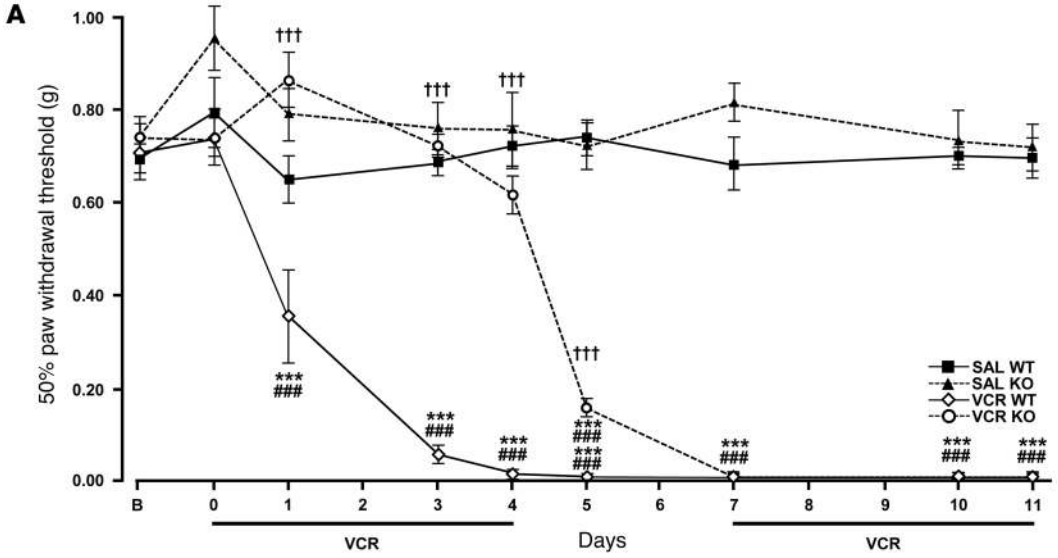

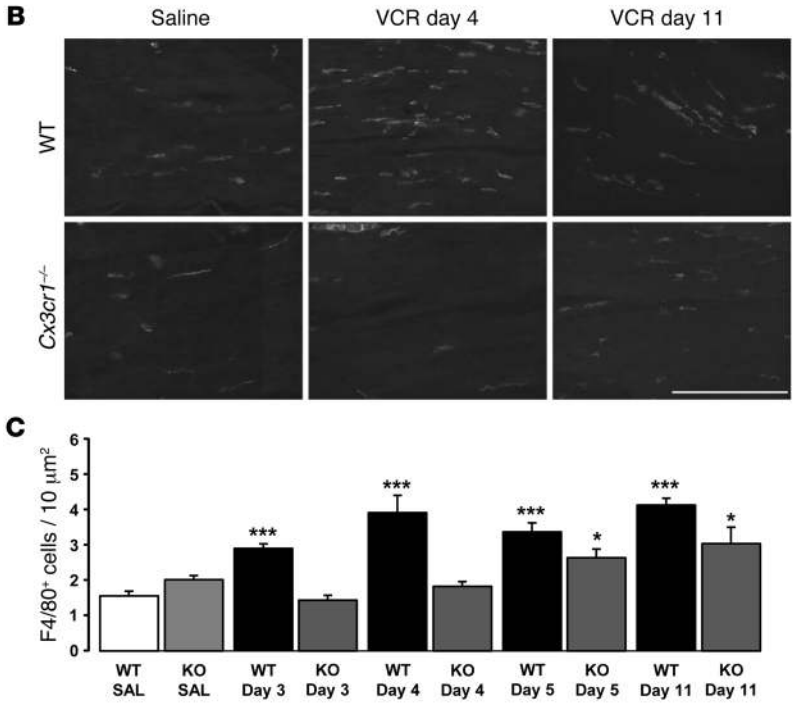

Figure 3
KO mice develop delayed allodynia following vincristine treatment. (**A**) Four-day delay of VCR-induced allodynia in KO mice compared with that in WT mice. Data are expressed as 50% of paw withdrawal thresholds (mean ± SEM, n = 8 mice in first VCR cycle [0.5 mg/kg/d i.p. from day 0 to day 4]; n = 4 mice in second VCR cycle [0.5 mg/kg/d i.p. from day 7 to day 11]). ***P < 0.001 compared to baseline thresholds, ###P < 0.001 compared to vehicle treated, †††P < 0.001 compared WT VCR treatment, 2-way RM ANOVA, post-hoc Holm-Sidak test. (**B**) Representative photomicrographs demonstrating reduced monocyte-macrophage (F4/80+ cell) infiltration in the sciatic nerves of KO mice compared with that in WT mice in the first VCR cycle (days 3 and 4) but not between cycles (day 5) and at end of second cycle (day 11). Scale bar: 200 μm. (**C**) The number of F4/80+ cells was counted in 10^4 μm^2 boxes in sciatic nerve segments (mean ± SEM, n = 4 mice per group). *P < 0.05, ***P < 0.001, 1-way ANOVA, post-hoc Tukey test.

suggest that the presence of the CX3CR1-expressing monocyte/macrophages population in the sciatic nerve is critical for the initial development of VCR allodynia.

The analysis of CX3CR1-expressing cells in the sciatic nerves of *Cx3cr1*$^{gpf/+}$ mice, in which the CX3CR1 receptor is tagged with green fluorescent protein, revealed that both GFP+ and F4/80+ cells were present in higher numbers following VCR treatment compared with that after saline treatment (Figure 4, A and B). Specifically, the number of F4/80+ cells increased 24 hours after VCR and remained significantly high following each of the 2 VCR cycles (Figure 4, A and B). A similar pattern of expression was observed using CD68 as a cell-specific marker (Supplemental Figure 7). However, the GFP+ cell number peaked 24 hours after the first VCR injection, was slightly reduced at the end of the first VCR cycle, and was significantly lower by the end of the second cycle (Figure 4, A and B). These data indicate that CX3CR1 monocytes populate the sciatic nerve immediately after the VCR treatment starts and during the first cycle but that they are less numerous afterward. Accordingly, VCR-induced allodynia did not manifest until the end of the first cycle in KO mice. As these mice showed no difference in dorsal horn microglial response compared with that of microglia from WT mice after 2 VCR cycles (Supplemental Figure 8), we can exclude the engagement of CX3CR1 microglial cells in response to VCR treatment. Therefore, even though the CX3CR1 receptor is also expressed by microglia in the CNS and activation of microglial CX3CR1 by neuronal FKN mediates pain

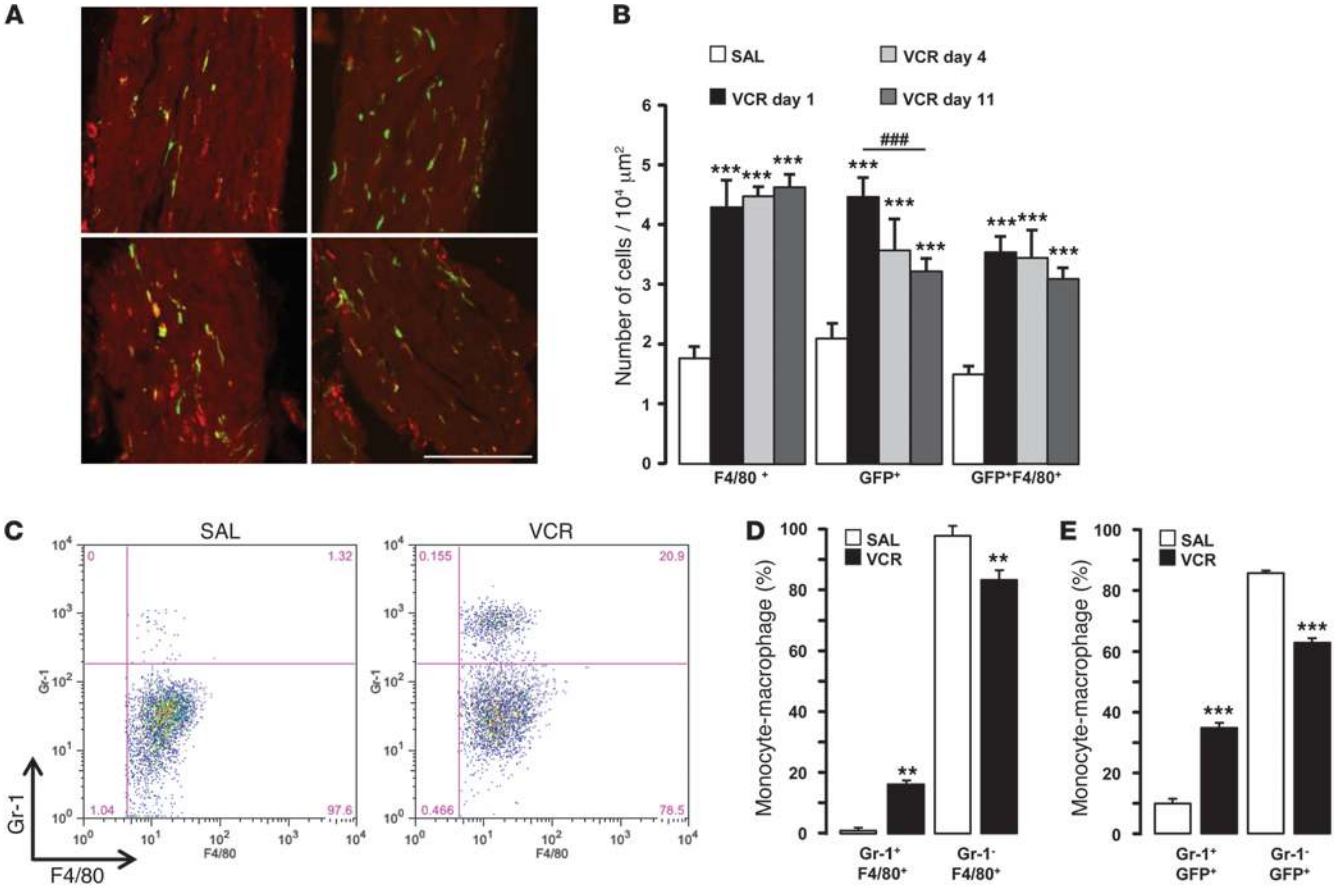

Figure 4

Vincristine treatment induces infiltration of CX3CR1 monocyte-macrophages in the sciatic nerve. (**A** and **B**) CX3CR1 monocyte-macrophages populate the sciatic nerve immediately after VCR treatment (day 1) and in the first cycle (days 0–4), but they are less numerous afterward (second cycle, days 7–11). (**A**) Representative photomicrographs showing CX3CR1-GFP$^+$ cells (green) and F4/80$^+$ cells (red) in sciatic nerve sections. Scale bar: 200 μm. (**B**) Positive cells were counted in 10^4 μm^2 boxes (mean ± SEM, $n = 4$ mice per group). ***$P < 0.001$ compared to saline, ###$P < 0.001$ VCR day 1 compared to VCR day 11, 1-way ANOVA, post-hoc Tukey test. (**C**–**E**) Peritoneal monocyte-macrophages express Gr-1 marker (proinflammatory phenotype) following the first cycle of VCR (day 4). (**C**) Dot plot analysis of Gr-1$^+$ and F4/80$^+$ peritoneal cells analyzed by flow cytometry. (**D**) Cumulative data for relative percentage of Gr-1$^+$ and Gr-1$^-$ cells in the F4/80$^+$ population; mean ± SEM of 3 WT mice treated with vehicle or VCR. **$P < 0.01$, 1-way ANOVA followed by Tukey post-hoc test. (**E**) Cumulative data for relative percentage of Gr-1$^+$ and Gr-1$^-$ cells in the GFP-positive population of *Cx3cr1*$^{gfp/+}$ mice; mean ± SEM of 3 mice treated with vehicle or VCR. ***$P < 0.001$, 1-way ANOVA followed by Tukey post-hoc test.

facilitation in the spinal cord after peripheral nerve damage (25), centrally located CX3CR1 receptors are not likely to be involved in VCR-induced allodynia.

Chemotherapeutic agents, including VCR, generally cause endothelial dysfunction (26) and, while showing tropism to peripheral sensory nerves, systemic VCR is likely to influence monocyte trafficking in other organs. Thus, in order to examine potential modulatory effects of VCR on monocyte-macrophage trafficking and/or phenotype, we characterized peritoneal cells after the first VCR cycle. While Gr-1$^-$F4/80$^+$ cells were detected in the peritoneal cavity of saline-treated mice, a prominent Gr-1$^+$F4/80$^+$ monocyte infiltrate was observed in VCR-treated animals (Figure 4, C and D). When relative percentages of Gr-1$^-$F4/80$^+$ and Gr-1$^+$F4/80$^+$ cells were quantified, a remarkable increase (~20-fold) in the latter population was measured in the VCR group (Figure 4D). The shift in the Gr-1–expressing monocyte-macrophage population induced by VCR treatment was also evident when *Cx3cr1*$^{gfp/+}$ mice were used, with an approximately 3-fold increase in Gr-1$^+$ cells (Figure 4E). These changes in relative percentages denote elevated numbers in the specific Gr-1$^+$ cell population, since the total number of peritoneal monocyte-macrophages was markedly elevated by treatment with VCR both in WT (from $3 \times 10^6 \pm 0.5 \times 10^6$ to $5.4 \times 10^6 \pm 0.4 \times 10^6$ cells in vehicle and VCR groups; $n = 3$, $P < 0.01$) and *Cx3cr1*$^{gfp/+}$ mice (from $4.5 \times 10^6 \pm 0.5 \times 10^6$ to $9.9 \times 10^6 \pm 1.6 \times 10^6$ cells in vehicle and VCR groups; $n = 3$, $P < 0.01$, Student's t test).

Our data up to this point form two key suggestions. First, CX3CR1$^+$ monocytes invade the sciatic nerve in concomitance to VCR-induced allodynia. Second, similarly to peritoneal Gr-1$^-$ monocytes, which shift toward a proinflammatory Gr-1$^+$ type during VCR treatment, in the sciatic nerve infiltrating monocyte-macrophages might promote inflammation and pain. Therefore, in the next two series of experiments, we investigated the underlying mechanisms for VCR-induced endothelial adhesion and transmigration of monocytes. We then evaluated whether monocyte-macrophages produce pronociceptive factors in a CX3CR1-dependent fashion.

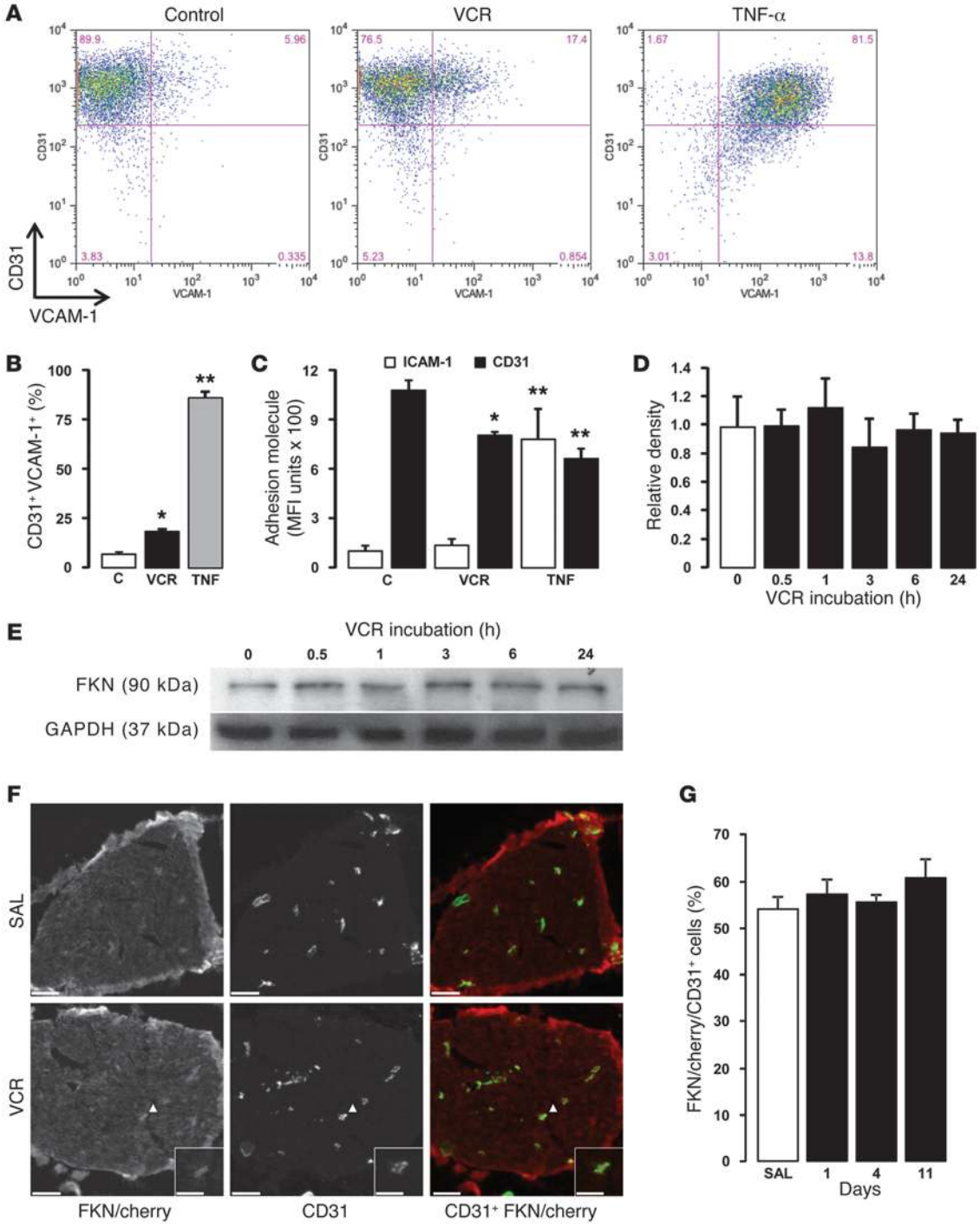

Figure 5

Vincristine treatment activates endothelial cells. (**A**–**C**) Expression of adhesion molecules VCAM-1 and ICAM-1 by primary HUVECs is increased by VCR (10 nM) or TNF-α (10 ng/ml) compared with control (cell media) following 18-hour incubation. (**A**) Representative plots for cells stained for CD31 and VCAM-1. (**B**) Cumulative data for CD31/VCAM-1 double-positive HUVECs. (**C**) ICAM-1 and CD31 levels on HUVECs. MFI, median fluorescence intensity (units). (**B** and **C**) Mean ± SEM of 3 distinct experiments. C, control, treated with media only. $^{*}P < 0.05$, $^{**}P < 0.001$ compared to saline, 1-way ANOVA followed by Tukey post-hoc test. (**D** and **E**) The expression of mature FKN protein in HUVECs is unchanged by incubation in VCR (10 nM for 30 minutes; $n = 3$ cultures). (**D**) Quantification of band density calculated using Bio-Rad's Quantity One software and normalized to GAPDH loading control. (**E**) Representative blot of FKN and GAPDH loading control in HUVEC lysates. (**F** and **G**) FKN expression by endothelial cells in vivo is unchanged by VCR treatment. (**F**) Representative photomicrographs showing expression of FKN-mCherry in CD31+ (endothelial) cells in transverse sciatic nerve sections obtained from *Cx3cl1mcherry* mice treated with either saline or 2 cycles of VCR. Scale bar: 100 μm; 50 μm (inset). (**G**) No change in (FKN)mcherry+CD31+ cells in the sciatic nerves after 1 day of VCR and at end of VCR cycles. The number of CD31+ cells that are positive for (FKN)mcherry was calculated following counting in whole nerve sections (mean ± SEM, $n = 4$ mice per group).

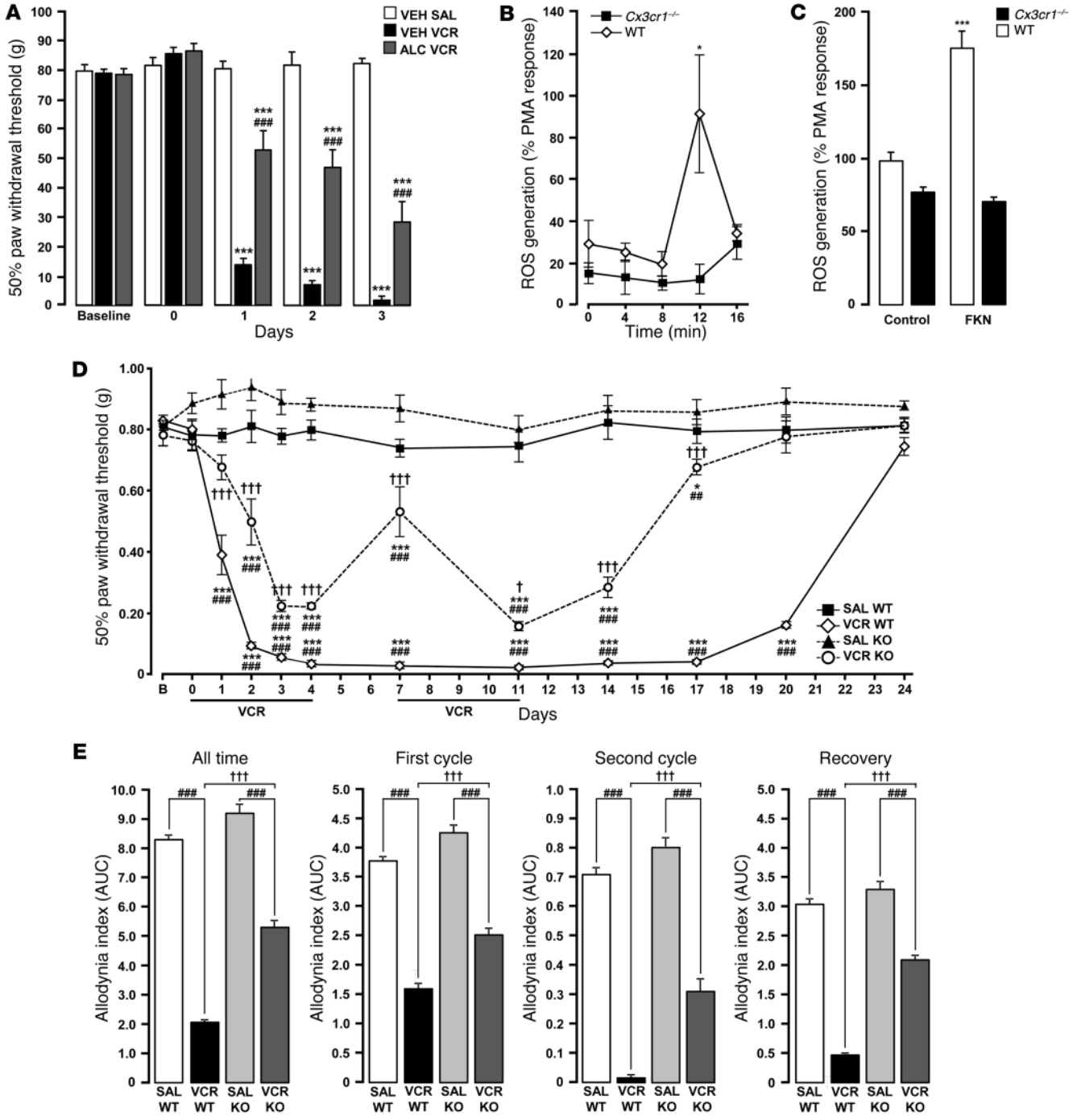

Figure 6

FKN triggers ROS production in CX3CR1 macrophages — a role for TRPA1 in VCR-induced allodynia. (**A**–**C**) FKN induces ROS production in macrophages; antioxidant treatment attenuates VCR-induced allodynia. (**A**) Acetyl-L-carnitine (ALC; 200 mg/kg twice a day) attenuates development of VCR-induced allodynia. Data are expressed as 50% paw withdrawal thresholds measured 1 hour after VCR (mean ± SEM, n = 10 mice per group). $^{***}P < 0.001$ compared to control (VEH SAL), $^{###}P < 0.001$ compared to VCR (VEH VCR), 2-way RM ANOVA, post-hoc Holm-Sidak. (**B** and **C**) FKN (mouse recombinant FKN [mrFKN]) 200 ng/ml) treatment of biogel-elicited macrophages from WT or KO mice induced ROS production in WT cells only. Data normalized to PMA at each time point (mean ± SEM, cells from 4 mice per group). $^{*}P < 0.05$, $^{***}P < 0.001$ compared to WT mice, 2-way ANOVA, Bonferroni post-hoc. (**B** and **C**) ROS generation, as measured by (**B**) bioluminescence following luminol (60 μm) incubation and by (**C**) fluorescence following DCFDA incubation (5 μM). (**D** and **E**) *Trpa1* KO mice develop less severe VCR-induced allodynia than WT mice. (**D**) Data are expressed as 50% paw withdrawal thresholds (mean ± SEM, n = 7 mice per VCR groups; n = 6 per saline group). $^{***}P < 0.001$ compared to baseline thresholds, $^{###}P < 0.001$ compared to vehicle treated, $^{†††}P < 0.001$ compared to WT VCR, 2-way RM ANOVA, post-hoc Holm-Sidak. (**E**) Allodynia index calculated as AUC from 0 to 24 days (ALL TIME); 0 to 4 days (First CYCLE); 7 to 11 days (Second CYCLE); 12 to 24 days (Recovery). Smaller area AUC represents greater allodynia (mean ± SEM, n = 7 mice per VCR groups, n = 6 mice per saline group). $^{###}P < 0.001$ compared to vehicle treated, $^{†††}P < 0.001$ compared to WT VCR treatment, 1-way ANOVA, post-hoc Holm-Sidak.

VCR and endothelial cells. We evaluated whether VCR can activate endothelial cells and quantified expression of selected adhesion molecules. We focused on ICAM-1 (CD54) and VCAM-1 (CD106), which are 2 integrin-binding endothelial cell adhesion molecules that play a fundamental role in the processes of monocyte intravascular crawling, firm adhesion to postcapillary venules, and migration in the subendothelial space (27–30). Incubation of primary HUVECs with VCR (10 nM) induced a significant increase of VCAM-1$^+$CD31$^+$ cells (Figure 5, A and B), as quantified at 18 hours by flow cytometry, with over a 3-fold increase over basal expression. No effects were observed at 4 hours (data not shown). Since ICAM-1 and CD31 (PECAM-1) are expressed by virtually all HUVECs, we measured expression of these adhesion molecules at the single cell level. Incubation of HUVECs with VCR produced a trend toward an increase in ICAM-1 expression on the cell surface, which was associated with a modest yet significant reduction (~20%) in CD31 expression (Figure 5C). The positive control, TNF-α, produced a marked increase in VCAM-1$^+$CD31$^+$ cells and ICAM-1 expression as well as a significant reduction in CD31 expression. We were not able to detect FKN cell surface expression by flow cytometry; however, Western blotting analysis revealed expression of mature FKN in HUVECs (Figure 5, D and E). Incubation with VCR (10 nM) for up to 24 hours did not alter cell-bound FKN (Figure 5, D and E). Similarly, in sciatic nerve sections in *FKNmCherry* mice, in which a BAC transgene harbors a FKN promoter–driven gene encoding a red fluorescent cherry reporter (31), mCherry$^+$ cells were found colocalized with the endothelial CD31 marker (by approximately 55%; Figure 5, E and F), in both saline- and VCR-treated nerves, expressing mCherry, thus confirming that FKN expression in endothelial cells in peripheral nerves is not altered by VCR. Collectively, these data indicate that VCR and TNF-α promote endothelial cell activation, albeit to a varying extent and with distinct profiles, and provide a mechanism by which VCR could facilitate endothelial-dependent trafficking of monocytes in the nerve.

Despite not being modulated by VCR, endothelial-bound FKN can contribute to the recruitment of circulating CX3CR1 monocytes (24). However, a more relevant function is likely to be played by shed FKN, proteolytically cleaved by ADAM10/17 or cathepsin S, which has been shown to promote transendothelial migration of CX3CR1 monocytes and proinflammatory monocyte activity in vascular diseases (24, 32).

CX3CR1-mediated ROS production and activation of neuronal TRPA1. In order to evaluate whether monocyte-macrophages produce pronociceptive mediators, we tested whether shed FKN induced production of pronociceptive reactive oxygen species (ROS), known to activate TRPA1 channels on the terminals of sensory neurons in sciatic nerve and evoke a pain response (33–35). Oxidative stress occurs during chemotherapy treatment, and TRPA1 receptors are an attractive pain target, as their antagonists attenuate established chemotherapy-induced mechanical and thermal hypersensitivity (36–38). Here, we observed that systemic treatment with the antioxidant acetyl-L-carnitine during the first VCR cycle significantly attenuated the development of allodynia by approximately 50% (Figure 6A), confirming the role of oxidative stress in the VCR model. Furthermore, treatment of macrophages with FKN at 200 ng/ml, but not 100 or 50 ng/ml (data not shown), induced rapid production of ROS that reached significance after 12 minutes of incubation (Figure 6, B and C). The effect of FKN was absent in KO macrophages (Figure 6, B and C), confirming the requirement of CX3CR1 receptor activation. The positive control phorbol 12-myristate 13-acetate (PMA) triggered ROS production to a similar extent to FKN at 12 minutes, yet the effect of PMA was sustained (up to 20 minutes) and consistent in both WT and KO macrophages (data not shown). Interestingly, the number of macrophages in the peritoneal wash of the KO mice ($9 \times 10^6 \pm 1.2 \times 10^6$) was significant lower than that in WT mice ($13.7 \times 10^6 \pm 0.7 \times 10^6$; $n = 3$ mice per group, $P < 0.05$, Student's t test), supporting the evidence that the CX3CR1 receptor affords nonredundant survival signals in these cells (23).

In the sciatic nerve, FKN-induced production of ROS from CX3CR1-expressing macrophages in the vicinity of sensory axons could result in a pronociceptive effect through the activation of TRPA1 receptors that are functionally located at axonal level (39–41). Thus, we demonstrated that 2 TRPA1 antagonists, AP-18 and A967079, repeatedly administered during the first VCR cycle, significantly prevented the development of VCR-induced allodynia by approximately 20% (Supplemental Figure 9). We then evaluated the profile of VCR-induced allodynia in *Trpa1* KO mice. We observed that *Trpa1* KO thresholds decreased following daily VCR administration but to a lesser extent than WT thresholds during the first VCR cycle (days 0–4), the 2-day pause period (days 5–7), and the second cycle (days 7–11) (Figure 6, D and E). In addition, the absence of TRPA1 resulted in faster recovery of thresholds after VCR withdrawal (days 12–24) (Figure 6, D and E). These data suggest that TRPA1 activation in peripheral nerves contributes to the development and, more significantly, to the maintenance of VCR-induced allodynia and TRPA1 channels are plausible candidates for mediating ROS pronociceptive effects.

Discussion

In this study, we have shown that VCR-induced allodynia is the result of a cascade of events, which start with an alteration in endothelial cell adhesion properties that promotes CX3CR1-expressing monocyte/macrophage trafficking into peripheral nerves. The recruitment of monocyte-macrophages and the activation of CX3CR1 receptor by endothelial FKN result in pronociceptive effects mediated by production of ROS and activation of TRPA1 channels in sensory neurons (Figure 7).

Our key observation in behavioral studies is that mice lacking the CX3CR1 receptor as well as a significant number of macrophages, as the absence of CX3CR1 could also hinder their survival, are refractory to the development of allodynia during the first of 2 VCR cycles. In addition, transient depletion of monocyte-macrophages by administration of LCL results in a similar delay in the development of allodynia during the first VCR cycle. This treatment is associated with up to 90% loss of both blood monocytes and splenic macrophages for 3 days and recovery of cell numbers after 8 days (19). Since all monocytes express CX3CR1 receptors, these observations indicate that CX3CR1-expressing monocyte-macrophages play a critical role in initiating VCR-induced neurotoxicity and pain.

Cancer treatment with chemotherapeutic agents is associated with peripheral neurotoxicity, which, although due to different mechanisms, remains a dose-limiting side effect for all agents. The incidence of neurotoxicity is variable and around 60% for VCR, which is used primarily for the treatment of hematological tumors. The mechanisms of neurotoxicity remain to be established. However, VCR, being a tubulin binder and microtubule inhibitor, induces disruption of axonal flow and distal axonopathy of the longest peripheral nerves in patients (1, 2, 42). Similarly, the mechanisms underlying pain development during cancer treatment are largely elusive. Preclinical models of

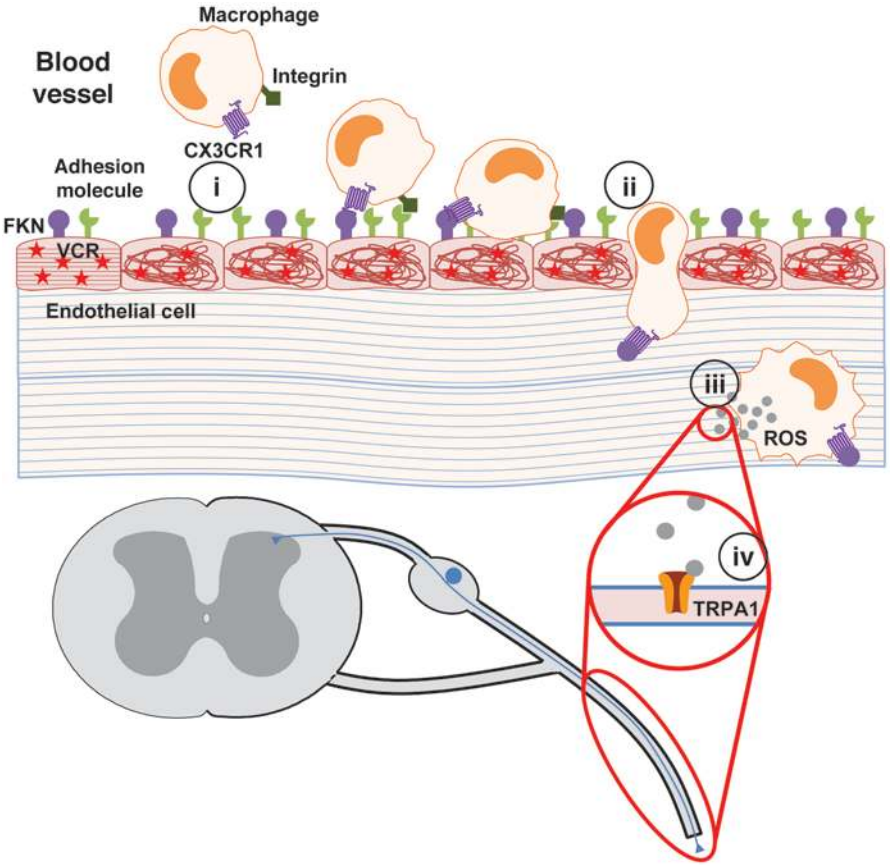

Figure 7
Novel pathway for vincristine-induced allodynia. VCR induces the expression of selected adhesion molecules, which promote monocyte trafficking (i). CX3CR1 monocyte-macrophages are recruited in the sciatic nerve following the same temporal pattern as VCR-induced allodynia (ii). Existing evidence suggests that CX3CR1 receptor interaction with endothelial-bound FKN results in transmigration of proinflammatory monocytes. Furthermore, FKN interaction with CX3CR1 in monocyte-macrophages promotes the formation of ROS (iii), which activate the TRPA1 channel in sensory neurons and evoke pain (iv).

cancer chemotherapy-induced neuropathies provide evidence for the development of mechanical and cold allodynia and some delayed loss of intraepidermal nerve fibers in the plantar skin of the rat hind paw (14) but neither peripheral nerve degeneration nor neuronal stress (9). Here, we observed no evidence of a loss of intraepidermal nerve fibers in the VCR mouse model, in line with previous observations (13). However, the infiltration of monocyte-macrophages into the nerve may be indicative of a subtle triggering event, occurring locally in the nerve, which remains to be defined. Sensory but not motor axons show slowed conduction velocities, and, in the spinal cord, central sensitization occurs with no concomitant microglial response (17, 18). Accordingly, we provide no evidence for sensory neuron damage and microglial activation in the dorsal horn following administration of VCR. Both the absence of microglial response and neuronal degeneration differentiate chemotherapy-induced allodynia from nerve-injury induced allodynia, which is associated with significant contribution of microglial-neuronal feedback to the chronicity of pain. Another intriguing observation is that, while microglial CX3CR1 receptors contribute to nerve injury–induced allodynia (25), centrally located CX3CR1 receptors are unlikely to participate to VCR-induced allodynia. Therefore, we can rule out a role for central CX3CR1 in VCR-induced allodynia and focus on the CX3CR1-expressing cells in the periphery, the monocyte-macrophage.

We observed that CX3CR1-GFP cells infiltrated the sciatic nerve as early as 24 hours after VCR administration and then their number gradually decreased by the end of the first VCR cycles. However, the number of $GFP^+F4/80^+$ cells in the sciatic nerve remained unchanged over the 2 VCR cycles. A plausible explanation is that the GFP^+ cells are $Ly6C^{hi}(Gr\text{-}1^+)CX_3CR1^{int}$ monocytes, which are recruited to the sciatic nerve within 24 hours from VCR administration. Such a setting in the sciatic nerve would resemble $Ly6C^{hi}(Gr\text{-}1^+)$ monocyte integration into the peritoneal macrophage pool, which occurs under inflammatory conditions (22). Moreover, the observed gradual decrease in GFP^+ population but constant presence of $F4/80^+$ cells throughout VCR treatment can be explained by the maturation of monocytes into macrophages, which are known to lose CX3CR1 expression but remain $F4/80^+$. In addition to the presence and absence of CX3CR1 expression, we provide evidence that infiltrating macrophages following VCR treatment can acquire a proinflammatory $Gr\text{-}1^+$ phenotype. This observation leads to the suggestion that monocyte-macrophages infiltrating the sciatic nerve can produce pronociceptive factors, which can activate neurons and evoke pain. Thus, at least initially, VCR administration does not cause detectable neuronal damage, but change is likely to occur within the microenvironment, inciting immune cell intervention, which mediates neuronal activation.

We have delineated a novel mechanism by which VCR promotes the transmigration of monocytes through the endothelium by showing, in flow cytometry experiments, that VCR induces the expression of selective adhesion molecules, which promote monocyte trafficking.

Together with chemoattractants, adhesion molecules are fundamental to promote extravasation of blood-borne immune cells at sites of tissue injury. Expressed at low levels in resting endothelia, adhesion molecules — such as selectins and immunoglobulin-like proteins — are rapidly upregulated in the early phases of the inflammatory response to bind their counter-receptors on the tethered leukocyte, assuring tissue-specific recruitment (28). VCR incubation with vascular endothelial cells provoked a significant, yet discreet when compared with the classical stimulus TNF-α, upregulation of VCAM-1 and ICAM-1. These adhesion molecules interact with β1 and β2 integrins to promote monocyte firm adhesion to postcapillary venules, migration across the endothelial wall, and locomotion into the subendothelial space (27). Although we show that VCR does not alter the expression of membrane-bound FKN in endothelial cells, current evidence show that, if not for cell adhesion, FKN-CX3CR1 interaction is key to promoting cell transmigration (24). Notably, shed FKN rather than membrane–bound FKN promotes monocyte infiltration in tissues (24), and endothelial FKN cleavage can be performed by endothelial ADAMs (23) or by cathepsin S (32) released by monocytes (19).

Besides promoting CX3CR1 monocyte transmigration, we show that FKN can induce transient generation of ROS by macrophages in a CX3CR1-dependent fashion. We postulate that ROS act as chemical mediator for immune-neuronal communication by activating transient receptor potential TRPA1 channels, which are functionally expressed by the axons of sensory neurons and evoke pain (33–35, 39, 40). Specifically, application of the selective TRPA1 activator mustard oil (MO) evokes depolarizing responses in murine isolated saphenous nerve. Surprisingly, MO loses efficacy in human isolated sural nerves, but this is very likely due to nerve exposure to local anesthetic during surgery. Indeed, lidocaine desensitizes murine TRPA1 channel, thereby suggesting that this mechanism, in combination with sodium channel blockade, underlies lidocaine efficacy in treating neuropathic pain (39). This is a plausible suggestion, as TRPA1-immunoreactive fibers are expressed in human peripheral nerves (41). Chemotherapeutic drugs increase oxidative stress, which may result in pain hypersensitivity following activation of TRPA1 and TRPV4 channels located on sensory neurons (36, 43, 44). Indeed, TRPV4 and TRPA1 receptor antagonists show good efficacy at preventing and attenuating oxaliplatin- and paclitaxel-induced neuropathic pain (36, 43). We have demonstrated that both an antioxidant agent and TRPA1 antagonists could also prevent VCR-induced pain. Furthermore, we observed a pronociceptive role for TRPA1 channels in the development and maintenance of VCR administration, as mice lacking this receptor developed less severe allodynia than controls and show quicker recovery after VCR withdrawal. Therefore, our data support the idea that oxidative stress and TRPA1 activation contribute to pain generation during chemotherapy. However, we have identified the monocyte-macrophages infiltrating in the sciatic nerve as the cellular source for ROS that activate neuronal TRPA1, thereby acting as mediator of immune-neuronal communication.

We have identified a possible mechanism by which VCR neurotoxicity occurs: a local effect at the endothelial-nerve interface that involves endothelial FKN- and CX3CR1-expressing monocytes and results in significant activation of pain transmission. Specifically, FKN, released by endothelial cells following proteolytic cleavage, is known to elicit CX3CR1 monocyte transmigration toward a subtly damaged neuronal axon, is able to promote production of pronociceptive ROS mediators, which constitute the endogenous ligands for the TRPA1 receptors expressed by nociceptive neurons. Altogether, these results support the proposal that TRPA1 antagonists would be beneficial in the treatment of chemotherapy-induced pain by reducing the severity of pain and accelerating its recovery.

The novelty of our study is in providing new therapeutic cues for the prophylactic treatment of chemotherapy-induced painful neuropathy, which can be considered an "orphan condition" if one considers the lack of valid therapeutic options. We suggest that CX3CR1 receptor antagonists and blockade of endothelial FKN solubilization by ADAM10/17 and/or cathepsin S inhibitors constitute new targets for pain prophylaxis in chemotherapy treatments. Relevantly, the first-in-class generation of CX3CR1 antagonists has been reported recently, and they include both brain and non-brain penetrant molecules for future pharmacological characterization (45). We are aware that the CX3CR1 receptor is expressed by cells other than macrophages, including dendritic cells and lymphocytes. CX3CR1 deficiency in the KO mice is associated with enhanced susceptibility to *Salmonella typhimurium* infection, due to reduced pathogen clearance by lamina propria dendritic cells (46). However, CX3CR1 expression on dendritic cells remains controversial (47), and compensatory/altered mechanisms and processes may occur in the global deficient mouse. Furthermore, it is not known whether acute inhibition of CX3CR1, using antagonists, would alter the tolerogenic environment within the small intestine. However, pharmacological inhibition of CX3CR1 with an antagonist might not necessarily be comparable to the phenotype of the knockout in terms of susceptibility to infection.

As both TRPA1 channels and CX3CR1 receptors are expressed peripherally, receptor antagonist and protease inhibitor molecules can be synthesized to be non-brain penetrant, thereby avoiding undesirable CNS effects.

Methods

Animals

Transgenic mice were produced using heterozygous breeding pairs to give litters of mixed genotypes, including KO animals, WT control animals, and heterozygous animals. For all experiments, unless otherwise stated, adult male and female mice were used (25–30 g, corresponding to 10 to 16 weeks of age). Male and female mice were found to have equivalent thresholds in all behavioral tests. C57BL/6J mice were obtained from Harlan UK.

For the production of KO animals, an original breeding stock was obtained from Taconic, where they had been generated on a C57BL/6 background, as previously described (48). Disruption of the *Cx3cr1* gene was confirmed using PCR and standard agarose gel electrophoresis with primers previously published (48). For the production of *Cx3cl1-mCherry* heterozygous mice, an original breeding stock was gifted by Steffen Jung, Department of Immunology, Weizmann Institute of Science, Rehovot, Israel. The *Cx3cl1-mcherry* heterozygous mice were generated using a RedET recombination system to replace the first exon of the *Cx3cl1* gene with a gene encoding a monomeric mCherry reporter gene and backcrossed onto a C57BL/6 background, as previously described (31). Expression of the *Cx3cl1-mCherry* gene was confirmed using PCR and standard gel electrophoresis with primers previously published (31). For the pro-

duction of *Cx3cr1-gfp* heterozygous mice, an original breeding stock was gifted by Steffen Jung. The *CX3cr1-gfp* heterozygous mice were generated using a CreLox recombination system to replace the first 390 bp of the *Cx3cr1* gene with a GFP-neo cassette. Mice were generated on a C57BL/6 background, and expression of the GFP was confirmed using PCR and standard gel electrophoresis with primers previously published (49). *Trpa1* KO mice and WT littermates were bred from heterozygous mice provided by Kelvin Kwan and David Corey (Harvard Medical School, Boston, Massachusetts, USA) and subsequently backcrossed for 10 generations onto a C57BL/6J background.

Animal husbandry and experiments were performed in a nonsterile housing environment in accordance with the United Kingdom Animals (Scientific Procedures) Act 1986 and local animal care and use guidelines.

Animals were randomly assigned to treatment groups so that each group contained approximately equal numbers of age-matched WT and KO mice of both sexes. For all studies, the experimenter was blind to genotype and treatment.

Behavioral testing

Animals were housed individually for 1 week prior to behavioral experiments to prevent aggressive behavior. Three baseline measurements were made prior to treatment, the average of which is presented. Static mechanical withdrawal thresholds were assessed by applying von Frey filaments (Linton Instruments) to the plantar surface of the hind paw (25, 32). Unrestrained animals were acclimatized in acrylic cubicles (8 × 5 × 10 cm) above a wire mesh for up to 60 minutes prior to testing. Calibrated von Frey filaments (0.008–1.4 g) (flexible nylon fibers of increasing diameter that exert defined levels of force) were applied to the plantar surface of the hind paw of the mouse until the fiber bent and then were held in place for 3 seconds or until the paw was withdrawn in a reflex not associated with movement or grooming. Filaments were applied alternately to the left and right hind paws. A 50% paw withdrawal threshold was calculated using the "up-down" method starting with the 0.6-g filament. If a positive response was observed, the next lower force hair was applied, and, if a negative response was observed, the next higher force hair was applied. Four subsequent hairs were then assessed according to the up-down sequence. Data are expressed as 50% paw withdrawal threshold in grams.

Vincristine treatment

VCR (Sigma-Aldrich) was dissolved in sterile saline, and 0.5 mg/kg VCR was injected into the peritoneal cavity (i.p.) using a 30-gauge needle. VCR was administered for two 5-day cycles (days 0–4 and 7–11) with a 2-day break between cycles, as previously described (11).

Macrophage depletion

Prior to vincristine treatment, the circulating monocyte/macrophage population was depleted, as described previously (19, 50). LCL (10 μl/g of a 5 mg/ml solution [Rooijen]) or control liposome-encapsulated PBS was administered to mice on 2 occasions, 3 and 1 days prior to VCR treatment, via injection into the peritoneal cavity with a 30-gauge needle.

TRPA1 antagonist/antioxidant treatment

TRPA1 antagonists AP-18 (Tocris) and A967079 (Tocris) were suspended in ddH_2O containing 0.5% methylcellulose (Sigma-Aldrich) and 0.5% Tween-80 (VWR). Antagonists (or vehicle) were administered via oral gavage (100 mg/kg) twice daily with the first administration occurring 1 hour prior to VCR administration. The antioxidant acetyl-L-carnitine (Sigma-Aldrich) was dissolved in sterile saline and administered (200 mg/kg) via injection into the peritoneal cavity with a 30-gauge needle twice daily, with the first administration occurring 1 hour prior to VCR administration.

Immunohistochemistry

Mice, under pentobarbital anesthesia (sodium pentobarbital, 200 mg/ml [Euthatal; Merial Animal Health]), were transcardially perfused with saline solution, followed by 4% paraformaldehyde in 0.1 M phosphate buffer containing 1.5% picric acid. The lumbosacral spinal cord was exposed by laminectomy and the lumbar enlargement and L3, L4, and L5 DRG were excised. The sciatic nerves of the animal were exposed by incision midway up the thigh, and 10- to 20-mm segments were excised; plantar glabrous skin was excised from the hind paw. Tissues were post-fixed for 2 to 4 hours in the perfusion fixative before being cryoprotected in 20% sucrose in 0.1 M phosphate buffer at 4°C for a minimum of 72 hours. Following cryoprotection, tissues were embedded in optimum cutting temperature–embedding medium (OCT [VWR]) and frozen in liquid nitrogen. Tissue sections were cryostat cut (Bright Instruments) and thaw mounted onto glass microscope slides (VWR). Nerve sections were incubated for 1 hour in 3% BSA in PBS-Tx-Az (PBS containing 0.2% Triton-X [Sigma-Aldrich] and 0.1% sodium azide [Sigma-Aldrich]), before being incubated overnight with a rat anti-mouse F4/80 (1:200 [Abd Serotech]) or with a rat anti-mouse CD68 antibody (1:500 [Abcam]) and subsequently incubated for 2.5 hours with an anti-rat Alexa Fluor 546 secondary antibody (1:1,000 [Invitrogen, Molecular Probes]) to detect monocyte-macrophages. To detect neutrophils, nerve sections were incubated overnight with a rabbit anti-MPO antibody (1:50 [Abcam]) and subsequently incubated for 2.5 hours with an anti-rabbit Alexa Fluor 488 secondary antibody (1:1,000 [Invitrogen, Molecular Probes]). DRG sections were incubated overnight with rabbit anti-ATF3 (1:500 [Santa Cruz Biotechnology]) and mouse anti-B_{III}tubulin (1:1,000 [Promega]) primary antibodies and subsequently incubated for 2.5 hours with anti-mouse Alexa Fluor 488 (1:1,000 [Invitrogen, Molecular Probes]) and anti-rabbit Alexa Fluor 546 (1:1,000 [Invitrogen, Molecular Probes]) secondary antibodies. Alternatively, to detect monocyte-macrophages, DRG sections were incubated for 1 hour in 3% BSA in PBS-Tx-Az, before being incubated overnight with a rat anti-F4/80 (1:200 [Abd Serotech]) and mouse anti-B_{III}-tubulin (1:1,000 [Promega]) primary antibodies and subsequently incubated for 2.5 hours with anti-rat Alexa Fluor 488 (1:1,000 [Invitrogen, Molecular Probes]) and anti-mouse Alexa Fluor 546 (1:1,000 [Invitrogen, Molecular Probes]) secondary antibodies. Spinal cord sections were incubated overnight with an anti-Iba1 primary antibody (1:1,000 [WAKO]), before incubation with an anti-rabbit Alexa Fluor 488 secondary antibody (1:1,000 [Invitrogen, Molecular Probes]) for 2.5 hours. Plantar glabrous skin sections were embedded in paraffin wax, cut in 8-μm sections, incubated with rabbit anti-PGP9.5 (1:5,000 [Ultraclone Ltd.]) overnight after citric acid heat-induced epitope retrieval, and subsequently incubated for 2.5 hours with an anti-rabbit Alexa Fluor 954 secondary antibody (1:1,000 [Invitrogen, Molecular Probes]). Slides were coverslipped with Vectashield mounting media with DAPI (Vector Laboratories) and visualized under a Zeiss Axioplan 2 fluorescent microscope and a Zeiss LSM710 confocal microscope (Zeiss). The number of positive cells for each immunohistochemical marker was determined. Three boxes measuring 2.25×10^4 μm^2 were spaced equally across the superficial laminae of the dorsal horn for spinal cord sections, or 7 boxes measuring 10^4 μm^2 were spaced equally across the tissue for nerve sections. The number of cells positive for the given marker was counted. In skin sections, the number of $PGP9.5^+$ fibers crossing the basal membrane into the epidermis was determined for the entire length of the sample, and a fiber density was calculated per mm of tissue. Three tissue sections per animal were selected at random with experimental group blinded.

ROS generation

Macrophages from both WT and KO animals were seeded at 2×10^5 cells per well in 96-well plates (Nunc) and left to adhere in RPMI-1640 (GE Healthcare) with 10% serum at 37°C for 1 hour. Cells were washed with warm PBS (Invitrogen) and incubated with freshly prepared RPMI-1640 supplemented

with 10% serum containing 60 μM luminol (Sigma-Aldrich). Macrophages were then treated with either PMA (100 ng/ml [Sigma-Aldrich]) or FKN (200 ng/ml) (recombinant mouse FKN chemokine aa 25–105, R&D Systems). This concentration was chosen from pilot experiments with a 0.2- to 200-ng/ml range and found to be consistently active. Following addition of treatments, ROS detection was read on a Novostar plate reader (BMG Labtech) at 37°C. In separate experiments, 1×10^6 peritoneal macrophages from either colony were treated with or without 200 ng/ml FKN plus 5 μM H2DCFDA (dichlorofluorescin diacetate [Life Technologies]) for 10 minutes. Cells were subsequently washed and intracellular ROS generation was detected on a Novostar plate reader (BMG Labtech).

Monocyte, macrophage, and endothelial cell analyses by flow cytometry

All conjugated antibodies were obtained from eBioscience (Hatfield), unless otherwise stated.

Monocyte phenotype. Following cardiac puncture under anesthesia, whole blood aliquots (100 μl) from *Cx3cr1*$^{gfp/+}$ animals treated with 0.5 mg/kg VCR for 1 to 11 days were stained with APC-conjugated Gr-1 (clone RB6-8C5); flow cytometry analyses allowed identification of the leukocyte populations, and, following a gating strategy based on side and forward scatter profiles, fluorescence in the blue channel (APC) and green channel (GFP) was acquired to quantify Gr-1$^+$GFP$^-$ and Gr-1$^+$GFP$^+$ cell populations.

Macrophage phenotype. Macrophages from WT mice were stained with FITC-conjugated Gr-1 (clone RB6-8C5) and APC-conjugated F4/80 (clone BM8). Macrophages from *Cx3cr1*$^{gfp/+}$ mice were stained with APC-conjugated Gr-1. Additional cells were labeled with appropriate isotype controls. For the staining procedure, 1×10^6 cells labeled with above conjugated antibodies were incubated on ice for 30 minutes. Cells were then washed twice with PBS containing 1.5% BSA and resuspended prior to analysis by flow cytometry.

HUVEC phenotype. Use of HUVECs was approved by the East London and The City Local Research Ethics Committee (REC Ref 06/Q0605/40 ELCHA). Briefly, cells were seeded into 12-well plates coated with gelatin and left in DMEM 10% FCS overnight to reach confluence. HUVECs were then stimulated with either 10 ng/ml human TNF-α or 10 nM VCR for 18 hours. These parameters were chosen on pilot experiments, with VCR 100 nM and an incubation time of 4 hours yielding insufficient HUVEC activation. Following culture, cells were gently trypsinized, resuspended in complete Medium-199 (GE Healthcare), washed, and stained with PE-conjugated ICAM-1 (clone HA58), FITC-conjugated VCAM-1 (AbD Serotec, clone 1.G11B1), or PE-conjugated CD31 (Biolegend, clone WB59) plus appropriate isotype controls. Cells were incubated on ice for 30 minutes and then washed twice with PBS containing 1.5% BSA and resuspended for analysis on the flow cytometer. In all cases, 20,000 events were acquired by using a FACSCalibur flow cytometer (Becton Dickinson) and analyzed using FlowJo analysis software (version 9.4.1.1, Treestar Inc.).

FKN Western blotting. A primary HUVEC line was obtained from HPA cultures. Cells were maintained in DMEM containing 40% HAM-12, 20% FBS, 1% penicillin/streptomycin (all Invitrogen) and containing 50 mg heparin (Sigma-Aldrich) and 25 mg EC mitogen (AbD Serotec) per liter.

For experiments, cells were grown to confluency on 6-well plates (Nunc) before being treated with VCR 10 nM in serum-free media. Protein lysates were collected by incubating the cells in lysis buffer consisting of 20 mM tris(hydroxymethyl)aminomethane (Sigma-Aldrich) pH 7.5; 10 mM NaF (Sigma-Aldrich); 150 mM NaCl (VWR); 1% nonyl-phenoxylpolyethoxylethanol (Sigma-Aldrich); 1 mM phenylmethanesulfonyl fluoride (Sigma-Aldrich); 1 mM Na_3VO_4 (Sigma-Aldrich); and 10 mg/ml proteinase inhibitor (Roche) on ice for 30 minutes. The plates were scraped and the lysates collected. These were then centrifuged at 100,000 *g* for 15 minutes at 4°C, and the supernatant was collected. Protein concentration of samples was determined using a BCA protein assay (Pierce). 25 μg protein was loaded per lane and separated on a 12% SDS-PAGE gel. After transfer, the blots were incubated overnight at 4°C with a polyclonal goat anti-human FKN antibody (1:500 [R&D Systems]), before being further incubated with a HRP-conjugated secondary antibody (anti-goat HRP, 1:2,000 [DAKO]) at room temperature for 1 hour. The blots were visualized by development with ECL solution (GE Healthcare) and exposed to Hyperfilm (GE Healthcare). The blots were then stripped of their initial antibody probe by incubation in TBS-T containing 1% SDS and 0.1% β-mercaptoethanol for 30 minutes at 60°C and reprobed for the loading control GAPDH, using a polyclonal rabbit anti-GAPDH antibody (1:1,000 [Sigma-Aldrich]). The blot was then incubated with an anti-rabbit HRP-conjugated secondary antibody (1:2,000 [DAKO]) and developed as before. The intensity of bands on the blots was analyzed using Bio-Rad's Quantity One software.

Statistics

All data were analyzed using SigmaPlot 12.0 (Systat Software Inc.). Behavioral data were analyzed by repeated-measures (RM) 2-way ANOVA, followed by Holm-Sidak test. Immunohistochemical and flow cytometric data were analyzed by 1-way ANOVA, followed by Tukey test. ROS production data were analyzed by 2-way ANOVA, followed by Bonferroni test. All data are shown as mean ± SEM, and data were considered significant where $P < 0.05$.

Study approval

All studies were carried out with appropriate ethical approval. Animal studies were performed in accordance with the United Kingdom Animals (Scientific Procedures) Act 1986 and local care and use guidelines. Approval for these studies was provided by King's Animal Welfare and Ethical Review Body, London, United Kingdom. The use of HUVECs for in vitro studies was approved by the East London and The City Local Research Ethics Committee (REC Ref 06/Q0605/40 ELCHA), London, United Kingdom.

Acknowledgments

E.A. Old was supported by a BBSRC CASE PhD studentship sponsored by Eli Lilly (grant reference BB/H531335/1). S. Nadkarni and M. Perretti acknowledge support from the William Harvey Research Foundation. We wish to thank Steffen Jung for fruitful discussion and Carl Hobbs and Tom Pitcher for technical support.

Received for publication June 3, 2013, and accepted in revised form February 21, 2014.

Address correspondence to: Marzia Malcangio, Wolfson CARD, King's College London, Guy's Campus, London Bridge, London SE1 1UL, United Kingdom. Phone: 04420.7848.6092; Fax: 04420.7848.6165; E-mail: marzia.malcangio@kcl.ac.uk.

1. Windebank AJ, Grisold W. Chemotherapy-induced neuropathy. *J Peripher Nerv Syst*. 2008;13(1):27–46.
2. Balayssac D, et al. Patterns of P-glycoprotein activity in the nervous system during vincristine-induced neuropathy in rats. *J Peripher Nerv Syst*. 2005; 10(3):301–310.
3. Kim BJ, et al. Chemotherapy-related polyneuropathy may deteriorate quality of life in patients with B-cell lymphoma. *Qual Life Res*. 2010;19(8):1097–1103.
4. Dougherty PM, Cata JP, Cordella JV, Burton A, Weng HR. Taxol-induced sensory disturbance is characterized by preferential impairment of myelinated fiber function in cancer patients. *Pain*. 2004;109(1–2):132–142.
5. Bennett BK, Park SB, Lin CS, Friedlander ML, Kiernan MC, Goldstein D. Impact of oxaliplatin-induced neuropathy: a patient perspective. *Support Care Cancer*. 2012;20(11):2959–2967.
6. Dougherty PM, Cata JP, Burton AW, Vu K, Weng HR. Dysfunction in multiple primary afferent fiber subtypes revealed by quantitative sensory testing in patients with chronic vincristine-induced pain. *J Pain Symptom Manage*. 2007;33(2):166–179.
7. Authier N, et al. Animal models of chemother-

apy-evoked painful peripheral neuropathies. *Neurotherapeutics*. 2009;6(4):620–629.
8. Geis C, Beyreuther BK, Stohr T, Sommer C. Lacosamide has protective disease modifying properties in experimental vincristine neuropathy. *Neuropharmacology*. 2011;61(4):600–607.
9. Flatters SJ, Bennett GJ. Ethosuximide reverses paclitaxel- and vincristine-induced painful peripheral neuropathy. *Pain*. 2004;109(1–2):150–161.
10. Peters CM, et al. Intravenous paclitaxel administration in the rat induces a peripheral sensory neuropathy characterized by macrophage infiltration and injury to sensory neurons and their supporting cells. *Exp Neurol*. 2007;203(1):42–54.
11. Hansen N, et al. Serotonin transporter deficiency protects mice from mechanical allodynia and heat hyperalgesia in vincristine neuropathy. *Neurosci Lett*. 2011;495(2):93–97.
12. Kiguchi N, Maeda T, Kobayashi Y, Kondo T, Ozaki M, Kishioka S. The critical role of invading peripheral macrophage-derived interleukin-6 in vincristine-induced mechanical allodynia in mice. *Eur J Pharmacol*. 2008;592(1–3):87–92.
13. Uceyler N, et al. Heterozygous P0 deficiency protects mice from vincristine-induced polyneuropathy. *J Neurosci Res*. 2006;84(1):37–46.
14. Xiao WH, Zheng H, Bennett GJ. Characterization of oxaliplatin-induced chronic painful peripheral neuropathy in the rat and comparison with the neuropathy induced by paclitaxel. *Neuroscience*. 2012;203:194–206.
15. Aapro MS, et al. EORTC guidelines for the use of granulocyte-colony stimulating factor to reduce the incidence of chemotherapy-induced febrile neutropenia in adult patients with lymphomas and solid tumours. *Eur J Cancer*. 2006;42(15):2433–2453.
16. Ransohoff RM, Perry VH. Microglial physiology: unique stimuli, specialized responses. *Annu Rev Immunol*. 2009;27:119–145.
17. Zheng FY, Xiao WH, Bennett GJ. The response of spinal microglia to chemotherapy-evoked painful peripheral neuropathies is distinct from that evoked by traumatic nerve injuries. *Neuroscience*. 2011;176:447–454.
18. Zhang H, Yoon SY, Zhang H, Dougherty PM. Evidence that spinal astrocytes but not microglia contribute to the pathogenesis of Paclitaxel-induced painful neuropathy. *J Pain*. 2012;13(3):293–303.
19. Barclay J, et al. Role of the cysteine protease cathepsin S in neuropathic hyperalgesia. *Pain*. 2007; 130(3):225–234.
20. Auffray C, et al. Monitoring of blood vessels and tissues by a population of monocytes with patrolling behavior. *Science*. 2007;317(5838):666–670.
21. Geissmann F, Jung S, Littman DR. Blood monocytes consist of two principal subsets with distinct migratory properties. *Immunity*. 2003;19(1):71–82.
22. Yona S, et al. Fate mapping reveals origins and dynamics of monocytes and tissue macrophages under homeostasis. *Immunity*. 2013;38(1):79–91.
23. Landsman L, et al. CX3CR1 is required for monocyte homeostasis and atherogenesis by promoting cell survival. *Blood*. 2009;113(4):963–972.
24. Schwarz N, et al. Requirements for leukocyte transmigration via the transmembrane chemokine CX3CL1. *Cell Mol Life Sci*. 2010;67(24):4233–4248.
25. Staniland AA, et al. Reduced inflammatory and neuropathic pain and decreased spinal microglial response in fractalkine receptor (CX3CR1) knockout mice. *J Neurochem*. 2010;114(4):1143–1157.
26. Michaelis M, et al. Chemotherapy-associated angiogenesis in neuroblastoma tumors. *Am J Pathol*. 2012;180(4):1370–1377.
27. Schenkel AR, Mamdouh Z, Muller WA. Locomotion of monocytes on endothelium is a critical step during extravasation. *Nat Immunol*. 2004;5(4):393–400.
28. Shi C, Pamer EG. Monocyte recruitment during infection and inflammation. *Nat Rev Immunol*. 2011;11(11):762–774.
29. White GE, Iqbal AJ, Greaves DR. CC chemokine receptors and chronic inflammation — therapeutic opportunities and pharmacological challenges. *Pharmacol Rev*. 2013;65(1):47–89.
30. Mamdouh Z, Chen X, Pierini LM, Maxfield FR, Muller WA. Targeted recycling of PECAM from endothelial surface-connected compartments during diapedesis. *Nature*. 2003;421(6924):748–753.
31. Kim KW, et al. In vivo structure/function and expression analysis of the CX3C chemokine fractalkine. *Blood*. 2011;118(22):e156–e167.
32. Clark AK, et al. Inhibition of spinal microglial cathepsin S for the reversal of neuropathic pain. *Proc Natl Acad Sci U S A*. 2007;104(25):10655–10660.
33. Andersson DA, Gentry C, Moss S, Bevan S. Transient receptor potential A1 is a sensory receptor for multiple products of oxidative stress. *J Neurosci*. 2008;28(10):2485–2494.
34. Dai Y, et al. Sensitization of TRPA1 by PAR2 contributes to the sensation of inflammatory pain. *J Clin Invest*. 2007;117(7):1979–1987.
35. Obata K, et al. TRPA1 induced in sensory neurons contributes to cold hyperalgesia after inflammation and nerve injury. *J Clin Invest*. 2005;115(9):2393–2401.
36. Trevisan G, et al. Novel therapeutic strategy to prevent chemotherapy-induced persistent sensory neuropathy by TRPA1 blockade. *Cancer Res*. 2013;73(10):3120–3131.
37. Chen Y, Yang C, Wang ZJ. Proteinase-activated receptor 2 sensitizes transient receptor potential vanilloid 1, transient receptor potential vanilloid 4, and transient receptor potential ankyrin 1 in paclitaxel-induced neuropathic pain. *Neuroscience*. 2011;193:440–451.
38. Barriere DA, et al. Paclitaxel therapy potentiates cold hyperalgesia in streptozotocin-induced diabetic rats through enhanced mitochondrial reactive oxygen species production and TRPA1 sensitization. *Pain*. 2012;153(3):553–561.
39. Docherty RJ, Ginsberg L, Jadoon S, Orrell RW, Bhattacharjee A. TRPA1 insensitivity of human sural nerve axons after exposure to lidocaine. *Pain*. 2013;154(9):1569–1577.
40. Weller K, Reeh PW, Sauer SK. TRPV1, TRPA1, and CB1 in the isolated vagus nerve — axonal chemosensitivity and control of neuropeptide release. *Neuropeptides*. 2011;45(6):391–400.
41. Anand U, et al. TRPA1 receptor localisation in the human peripheral nervous sytem and functional studies in cultured human and rat sensory neurons. *Neurosci Lett*. 2008;438(2):221–227.
42. Balayssac D, et al. Chemotherapy-induced peripheral neuropathies: from clinical relevance to preclinical evidence. *Expert Opin Drug Saf*. 2011;10(3):407–417.
43. Alessandri-Haber N, Dina OA, Joseph EK, Reichling DB, Levine JD. Interaction of transient receptor potential vanilloid 4, integrin, and SRC tyrosine kinase in mechanical hyperalgesia. *J Neurosci*. 2008;28(5):1046–1057.
44. Flatters SJ, Bennett GJ. Studies of peripheral sensory nerves in paclitaxel-induced painful peripheral neuropathy: evidence for mitochondrial dysfunction. *Pain*. 2006;122(3):245–257.
45. Karlstrom S, et al. Substituted 7-amino-5-thiothiazolo[4,5-d]pyrimidines as potent and selective antagonists of the fractalkine receptor (CX3CR1). *J Med Chem*. 2013;56(8):3177–3190.
46. Niess JH, et al. CX3CR1-mediated dendritic cell access to the intestinal lumen and bacterial clearance. *Science*. 2005;307(5707):254–258.
47. Medina-Contreras O, et al. CX3CR1 regulates intestinal macrophage homeostasis, bacterial translocation, and colitogenic Th17 responses in mice. *J Clin Invest*. 2011;121(12):4787–4795.
48. Combadiere C, et al. Decreased atherosclerotic lesion formation in CX3CR1/apolipoprotein E double knockout mice. *Circulation*. 2003;107(7):1009–1016.
49. Jung S, et al. Analysis of fractalkine receptor CX(3) CR1 function by targeted deletion and green fluorescent protein reporter gene insertion. *Mol Cell Biol*. 2000;20(11):4106–4114.
50. Van Rooijen N, Sanders A. Liposome mediated depletion of macrophages: mechanism of action, preparation of liposomes and applications. *J Immunol Methods*. 1994;174(1–2):83–93.